Reprinted from SPIE Vol. 637—Ocean Optics VIII

Effects of sensor characteristics on the inferred vertical structure of the diffuse attenuation coefficient spectrum

D.A. Siegel

Ocean Physics Group
Department of Geological Sciences
University of Southern California
Los Angeles, California 90089-0741

C.R. Booth

Biospherical Instruments, Inc.
4901 Morena Boulevard, #1003
San Diego, California 92117

T.D. Dickey

Ocean Physics Group
Department of Geological Sciences
University of Southern California
Los Angeles, California 90089-0741

Abstract

A series of model calculations illustrate how the spectral characteristics of an irradiance sensor can affect estimates of the vertical structure of the diffuse attenuation coefficient for downwelling irradiance ($K(z,\lambda)$). The effect of a finite spectral response function is observed in regions of the spectrum where large dispersive changes exist in the optical properties. For open ocean environments, this occurs in the orange-red region of the spectrum (λ>550nm).

Four model calculations are made using different spectral response functions ($h(\lambda)$) to determine the effects on the inferred K(z,625nm) profiles related to: 1) a finite bandpass, 2) the "leakage" of a finite amount of blue-green light, 3) spectral tails, and 4) a spectral response function measured with a spectroradiometer. The results of these model calculations indicate that the background irradiance (or equivalently the blocking level) sampled by the spectroradiometer must be less than 10^{-6}% (or 8 orders of magnitude) of the irradiance of interest for an accurate estimate of $K(z,\lambda)$. Also, the half power bandwidth of $h(\lambda)$ should be 10nm or less. The model results are compared to observed vertical profiles of $K(z,\lambda)$ sampled from the R/P FLIP in the North Pacific Ocean during the Optical Dynamics Experiment (ODEX). These calculations illustrate the possible implications of inappropriate sensor design on the interpretation of observed $K(z,\lambda)$ profiles.

Introduction

The determination of the diffuse attenuation coefficient ($K(z,\lambda)$) is important for the characterization of the underwater photo-environment. $K(z,\lambda)$ quantitatively describes the attenuation with depth of a diffuse beam of light. The downwelling spectral irradiance at depth can be evaluated given the vertical profile of $K(z,\lambda)$ and the downwelling spectral irradiance just beneath the air-sea interface ($E_d(0^-,\lambda)$) using the Beer-Bouguer-Lambert relation,

$$E_d(z,\lambda)=E_d(0^-,\lambda)e^{-\int_{0^-}^{z} K(z',\lambda)dz'} \quad (1)$$

where z is depth below the sea surface. The characteristics of $K(z_o,\lambda)$ (where z_o is a depth near the sea surface) have been explored in many differing oceanic environments (e.g., Smith and Baker[1]; Austin and Petzold[2]), but a characterization of the vertical structure of $K(z,\lambda)$ is an important current research topic (e.g., Smith, et al.[3]; Siegel and Dickey[4]).

The determination of the vertical structure of $K(z,\lambda)$ has proven to be quite difficult and the subject of much investigation (i.e., Smith and Baker[5,6]; Mueller[7]; Voss, et al.[8]; Siegel and Dickey[4]). These investigations have been primarily concerned with variability of the incident and/or in situ irradiance fields caused by cloud variations, surface gravity waves, and ship shadowing. The present study focuses upon the effects which the

underwater irradiance sensor may have upon the inferred K(z,λ) profile. The inferred diffuse attenuation coefficient is defined as $K_s(z,\lambda_o;h(\lambda))$, where λ_o is the wavelength of interest and $h(\lambda)$ is a spectral response function of the irradiance sensor.

In practice, spectroradiometers must have finite spectral bandwidths in order to measure a finite spectral irradiance for each waveband of interest. Profiles of spectral irradiance sampled from a spectroradiometer can be used to calculate an observed $K(z,\lambda)$ ($K_{obs}(z,\lambda)$) for each waveband. The calculated $K_{obs}(z,\lambda)$ may deviate substantially from the actual $K(z,\lambda)$ due to the finite spectral extent of the spectroradiometer. This report will show how large deviations in the calculated $K_{obs}(z,\lambda)$ may occur because of the finite extent of the irradiance sensor. It will also be shown that these distortions will be most severe for spectral regions with the greatest changes in $K(z,\lambda)$ with wavelength.

The present research has been motivated to a large extent by an analysis of the downwelling spectral irradiance sampled from the R/P FLIP during the Optical Dynamics Experiment (ODEX). These data were taken in the fall of 1982 in the central North Pacific Ocean (~33N, ~142W). Profiles of downwelling spectral irradiance were made with a Biospherical Instruments, Inc. (BSI) MER-1010 spectroradiometer. These data were then used to calculate $K_{obs}(z,\lambda)$ for 12 discrete wavebands (from 410 to 767nm). Thirty-two downwelling irradiance casts deemed void of incident irradiance fluctuations were chosen for analysis. A discussion of the general experimental design and the details of the estimation of $K_{obs}(z,\lambda)$ can be found in Dickey, et al.[9] and Siegel and Dickey[4], respectively.

The mean near-surface spectrum of $K(5m,\lambda)$ is shown in Figure 1. This was constructed by linearly interpolating between the 11 discrete wavebands in the visible region of the mean $K(5m,\lambda)$ to 1 nm intervals and then smoothing the spectrum using a 10nm moving average. In the following calculations, this spectrum is assumed to be the "true" depth independent $K(\lambda)$. In particular, the dependence of the sensed $K(z,\lambda)$ ($K_s(z,\lambda;h(\lambda))$) upon the shape of the spectral response function of the downwelling irradiance sensor $h(\lambda)$ is investigated.

The mean ODEX near-surface diffuse attenuation coefficient spectrum shows a broad minimum region from about 410 to 500nm, which is consistent with most open ocean observations. For wavelengths greater than 575nm, the magnitude of $K(5m,\lambda)$ increases quite rapidly. Changes in the spectral content of the downwelling irradiance field become greater with increasing depth in this portion of the spectrum as well. It will be shown in the next section that the properties of $h(\lambda)$ alter the sampled irradiance and hence $K_s(z,\lambda_o;h(\lambda))$ in this region of the spectrum.

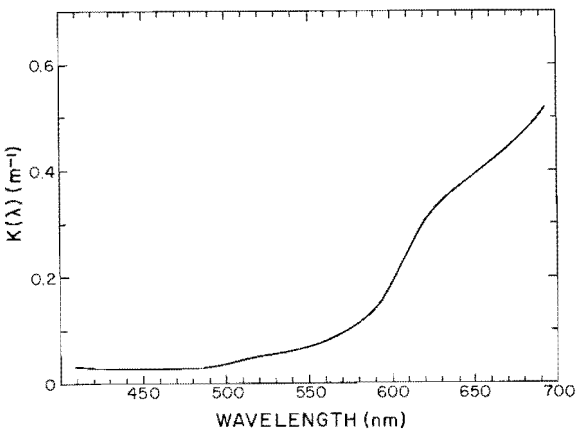

Figure 1: The mean near-surface $K(5m,\lambda)$ spectrum measured during ODEX from the R/P FLIP. Units are m^{-1}.

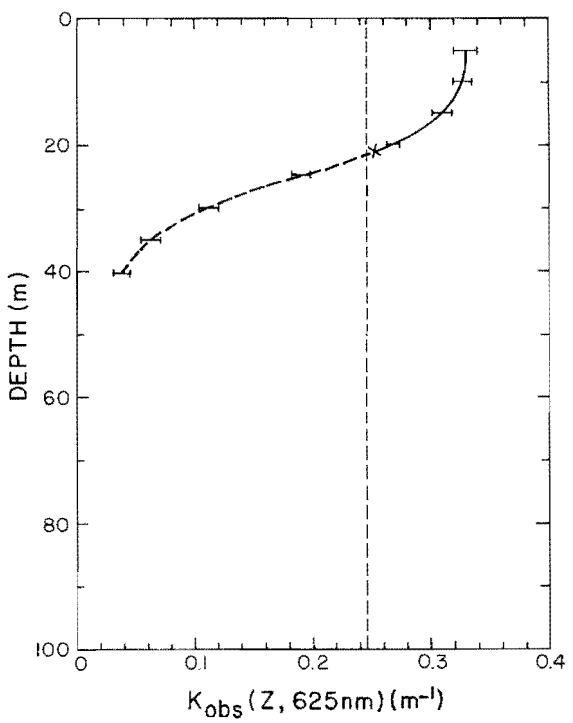

Figure 2: The mean observed $K(z,625nm)$ ($K_{obs}(z,625nm)$) from the R/P FLIP during ODEX. Units are m^{-1}. The 'X' represents the depth to which $K_{obs}(z,625nm)$ can be reasonably estimated, and the $K_{obs}(z,625nm)$ profile is dashed below this point. The error bars represent 95% confidence intervals for the mean $K_{obs}(z,625nm)$.

An example of an observed $K(z,\lambda)$ profile is shown for the 625nm waveband ($K_{obs}(z,625nm)$, Figure 2). This profile is constructed from the mean of the same 32 casts that were used to calculate the mean near-surface spectrum (Figure 1). The vertical dashed line corresponds to the diffuse attenuation coefficient for pure sea water at 625nm, ($K_w(625nm)$, Smith and Baker[1]). The calculation procedure used to determine $K_{obs}(z,625nm)$ is identical to the one suggested by Smith and Baker[5] except that the averaging and regression depth intervals were slightly larger (see Siegel and Dickey[4] for further details).

The magnitude of the observed diffuse attenuation coefficient decreases quite abruptly with increasing depth for this waveband, particularly for depths greater than ~20m. This trend of decreasing $K_{obs}(z,\lambda)$ was observed in all of the wavebands sampled by the spectroradiometer that were greater than 589nm. It should be indicated that observed water mass properties (i.e., temperature, salinity, chlorophyll-a concentration, in situ fluorescence, beam attenuation coefficient, etc.) were nearly uniform within the near-surface mixed layer (or upper 40 to 50m). The investigation of the cause(s) of the decrease in $K_{obs}(z,\lambda)$ with depth is what has motivated the present study.

The 'X' in Figure 2 (and in Figures 4, 6, and 8) represents the depth (for each waveband) below which one cannot reasonably estimate $K(z,\lambda)$ because of the finite dynamic range of the spectroradiometer. The method for determining this depth is as follows: 1) It is assumed that approximately 10 bits of information are required in order to calculate a vertical gradient of the downwelling irradiance (a conservative estimate), 2) the calibration constant is ~0.0001 $W/m^2/nm/bit$, and 3) $E_d(0^-,\lambda)$ is assumed to be ~1$W/m^2/nm$, thus by using the Beer-Bouguer-Lambert relation (eqn. 1) one can conservatively estimate $K(z,\lambda)$ over ~3 orders of magnitude of $E_d(z,\lambda)$ or approximately 7 optical depths. This depth is defined as z_x. $K_{obs}(z,\lambda)$ estimates below this depth are shown as dashed lines in Figure 2.

Several factors can cause the observed decrease of the magnitude of $K_{obs}(z,\lambda)$ with increasing depth. An internal source of light within the water column would make the water column appear to attenuate less light. A possible source of this background light field is sunlight induced fluorescence of the phytoplankton pigments (natural fluorescence) (e.g., Gordon[10]; Topliss[11]). For example, deep penetrating blue-green light can be absorbed by the phytoplankton and re-emitted as red light. This mechanism could in principle account for a reduction of the gradient of the red downwelling irradiance and hence a reduction of $K_{obs}(z,\lambda)$ with increasing depth. The possibility that these effects could be caused by characteristics of the irradiance sensor are considered in the next section.

Model

A simple model is introduced in order to develop some insight into the effects of a realistic irradiance sensor on the vertical structure of $K_{obs}(z,\lambda)$. This insight can be used to distinguish between sensor effects as opposed to effects caused by natural fluorescence. As the starting point for this model, the Beer-Bouguer-Lambert relation (eqn. 1) is used to relate the downwelling spectral irradiance at depth, $E_d(z,\lambda)$, to the downwelling irradiance just below the sea surface, $E_d(0^-,\lambda)$. The irradiance sampled by the underwater sensor is expressed as

$$E_s(z,\lambda_o;h(\lambda)) = \frac{\int_0^\infty h(\lambda)E_d(z,\lambda)d\lambda}{\int_0^\infty h(\lambda)d\lambda} \qquad (2)$$

where the spectral response function $h(\lambda)$ controls the amount and quality of the light sampled by the spectroradiometer and λ_o is the wavelength at the center of $h(\lambda)$. $K_s(z,\lambda_o;h(\lambda))$ is defined by an application of the Beer-Bouguer-Lambert relation for the

sampled irradiance,

$$E_s(z,\lambda_o;h(\lambda)) = E_s(0^-,\lambda_o;h(\lambda))e^{-\int_{0^-}^{z} K_s(z',\lambda_o;h(\lambda))dz'} \quad (3)$$

In this model, $K_s(z,\lambda_o;h(\lambda))$ can be calculated assuming that: 1) the downwelling irradiance spectrum just below the sea surface ($E_d(0^-,\lambda)$) is independent of the wavelength of light (i.e., $E_d(0^-,\lambda)=E_d(0^-)=E_s(0^-)$) and 2) the "true" $K(z,\lambda)$ is independent of depth (i.e., $K(z,\lambda)=K(\lambda)$). This then leads to the expression

$$K_s(z,\lambda_o;h(\lambda)) = \frac{\int_0^\infty K(\lambda)h(\lambda)e^{-K(\lambda)z}\,d\lambda}{\int_0^\infty h(\lambda)e^{-K(\lambda)z}\,d\lambda} \quad (4)$$

This equation states that the inferred $K(z,\lambda)$ profile is the "true" $K(z,\lambda)$, weighted by the in situ irradiance sampled by the irradiance sensor. Similar expressions are reported in Jerlov[12] for the centered wavelengths of colored glass filters, but do not account for the effects of filter shapes on an inferred optical property. This expression will be used in the calculation of $K_s(z,\lambda_o;h(\lambda))$ for three ideal types of spectral response functions and one realistic filter shape determined from measurements with a BSI spectroradiometer.

Analysis

Spectral response functions can be characterized by their bandwidth, the extent and magnitude of the tails, and by the magnitude of any anomalous spectral region through which light may still propagate. In the following, three ideal spectral response functions are used to determine how $K_s(z,625nm;h(\lambda))$ is affected by: 1) finite bandwidth, 2) stray blue-green light, and 3) spectral tails. Also, a measured $h(\lambda)$ function derived from a BSI spectroradiometer is utilized to examine its effect on the inferred vertical structure of $K(z,\lambda)$.

The idealized spectral response function of a finite bandpass filter is shown in Figure 3a. The center of the bandpass filter is λ_o and its spectral bandwidth is λ_b. $K_s(z,625nm;h(\lambda))$ can be calculated for various bandwidths. This calculation will give some insight into the effects of a finite bandpass $h(\lambda)$ on $K_s(z,625nm;h(\lambda))$.

The $K_s(z,625nm;h(\lambda))$ profiles for the finite bandpass case are shown in Figure 4a. As before, the 'X' represents the maximum depth to which one can reliably estimate $K(z,\lambda)$ using a BSI spectroradiometer (z_x). The dashed line is the mean ODEX near-surface K(625nm), which is assumed to be depth independent. It can be seen that the vertical structure of the inferred $K(z,\lambda)$ is strongly affected by the finite bandpass $h(\lambda)$ if the spectral bandwidth is greater than 10nm. There appears to be little variation from the assumed vertical structure to a depth of z_x if λ_b is less than 10nm. It is obvious that a great deal of sensor related vertical variation can exist if the bandwidth of the sensor is greater than 10nm (that of the BSI spectroradiometer).

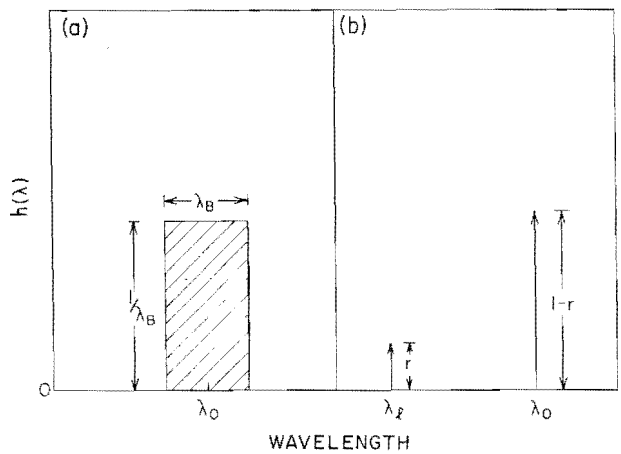

Figure 3: Hypothetical spectral response functions for a) finite bandpass $h(\lambda)$ and b) light leakage $h(\lambda)$. Units are arbitrary.

of the idealized stray light $h(\lambda)$ case may be quite important for
of the observed $K(z,\lambda)$ profiles ($K_{obs}(z,\lambda)$). Interference filt
tic irradiance sensors allow some small, though finite, level o
ectral regions that are designed to be devoid of light. T
are generally small ($O(10^{-4}\%$ or less) and are assumed to be in
magnitude of the sampled irradiance near the wavelength of int
ensor is profiled through the water column of the open ocean, t
irradiance field is altered because of the attenuation of the
is possible that at some depth the irradiance sampled by the se
ing level will be of similar magnitude as the irradiance samp
velength of interest. The fraction of stray light modeled by t
eptually related to this finite blocking level. Characterist
level will be discussed further in the context of a realist
n.

alized spectral response function to be considered pertains to
ils on the inferred $K(z,\lambda)$. An example of this type of sh
ty interference filter shown in Figure 5 (Melles Griot[13]). A

power bandwidth is used for these calculations. The value of n represents the number of individual metal coated dielectric filters which comprise the n-cavity interference filter. Each one of the metal coated dielectric filters reflects photons that are not in the waveband of interest, while allowing photons of

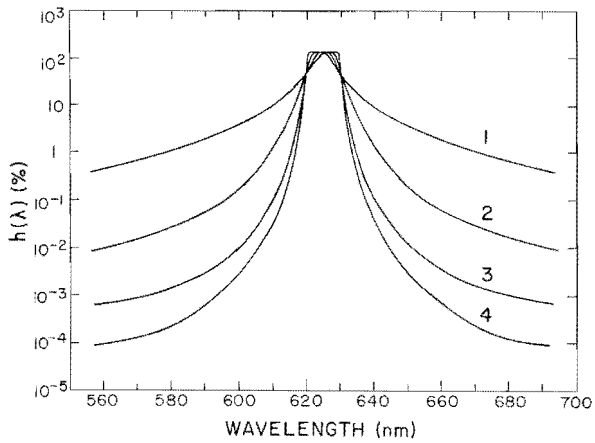

Figure 5: The shape of the spectral response functions for the idealized n-cavity interference filter case, where n varies from 1 to 4. Note the logarithmic scale. Units are % of full signal.

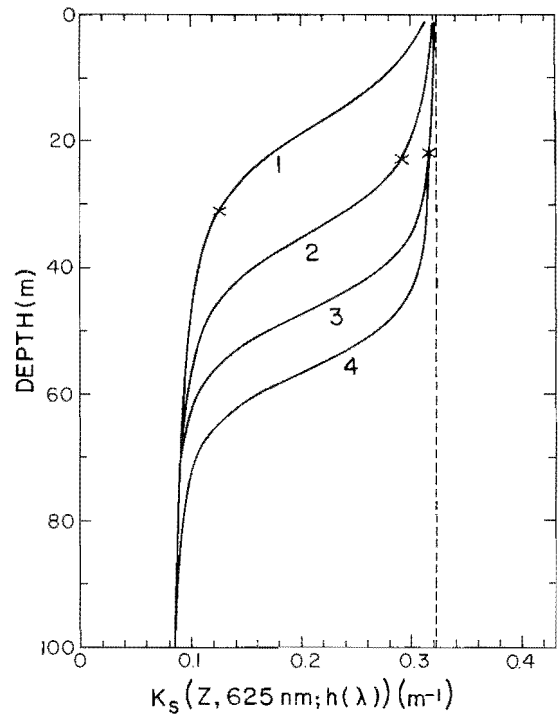

Figure 6: Inferred K(z,625nm) for the idealized n-cavity interference filter case. Units are m^{-1}.

interest to pass through. The inclusion of more of these cavities effectively sharpens the spectral region of $h(\lambda)$.

The $K_s(z,625nm;h(\lambda))$ profiles for the n-cavity interference filter $h(\lambda)$ are shown in Figure 6. At depths greater than 40m, all $K_s(z,625nm;h(\lambda))$ diverge from the assumed depth independent value of K(625nm) (the dashed line in Figure 6). At a depth of z_x, the 1 and 2 cavity interference filter cases diverge from K(625nm), while the 3 and 4 cavity cases do not. In general, the broader the spectral tails the more the $K_s(z,625nm;h(\lambda))$ diverge from the assumed depth independent value of K(625nm) (the dashed line in Figure 6). At a depth of z_x, the 1 and 2 cavity interference filter cases diverge from K(625nm), while the 3 and 4 cavity cases do not. In general, the broader the spectral tails the more the $K_s(z,625nm;h(\lambda))$ profile differs from the ideal sensor case. There also appears to be little advantage in using a 4 cavity interference filter opposed to a 3 cavity filter in that both $K_s(z,625nm;h(\lambda))$ profiles are identical to a depth of z_x.

The spectral response function measured for the 625nm waveband channel of a BSI spectroradiometer is shown in Figure 7. Because of the finite signal level of the monochrometer used to derive this $h(\lambda)$, the spectral response of the sensor was not sampled for $h(\lambda)$ less than 0.01%. Each spectral waveband of the BSI spectroradiometer utilizes a 3-cavity interference filter with additional colored glass filters in order to attenuate radiant energy outside of the desired waveband. Note that the center wavelength is 620nm. For these calculations, λ_o is assumed to be 620nm instead of λ_o=625nm. The shape of the spectral response function is different from the idealized $h(\lambda)$'s for the n-cavity interference filters (Figure 5). The sampled $h(\lambda)$ lacks an observable contribution from the spectral tails. Presumably, the tails of this $h(\lambda)$ have amplitudes less than 0.01%. Hence, calculations of $K_s(z,620nm;h(\lambda))$ using this $h(\lambda)$ have an inherent uncertainty due to the lack of knowledge of the low signal features of the spectral response function (i.e., the spectral tails and blocking level).

ical profile from the measured
are shown in Figure 8. Four
s are investigated. A background
king level is varied from 0 to
%. This blocking level is extend-
cross the entire visible spectrum
m 410 to 694nm). For all of the
s shown, $K_s(z,620nm;h(\lambda))$ diverges

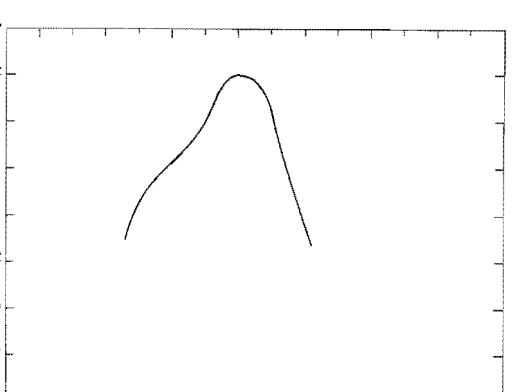

re 7: A realistic spectral re-
se function measured with a BSI
1010 spectroradiometer. Note

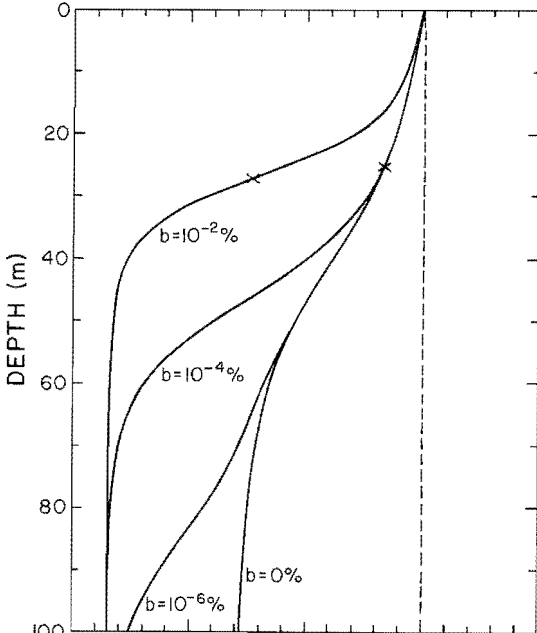

Figure 8: $K_s(z,620nm;h(\lambda))$ profiles
realistic spectral response function.
blocking level is also used for these

z,620nm,h(λ)) from the 0% blocking level case to a depth of 100m. These model
ch use a measured spectral response function clearly illustrate how the low
ions of h(λ) can help control the vertical structure of $K_s(z,620nm;h(\lambda))$ wh
ongly varies with wavelength. This analysis also shows that extreme care
rcised in the interpretation of observed K(z,λ) profiles.

Discussion

The preceding calculations illustrate the importance of the spectral respons
the determination of $K_s(z,\lambda_o;h(\lambda))$. The emphasis of this study is upon the
the visible spectrum characteristic of open ocean conditions, but it could
lied to any other spectral region where there exists large spectral gradients
perties. Conceptually, spectral response functions allow the sensor to s
x" light which is of interest with light that may not be desired. This of co
unambiguous interpretation of observed K(z,λ) profiles (i.e., Figure 2) dif
impossible.

The vertical structure of $K_{obs}(z,625nm)$ (Figure 2) is quite similar to the mod
ht $K_s(z,625nm;h(\lambda))$ with a stray fraction (r) of 0.01% (Figure 4b) and is al
the realistic h(λ) with a finite blocking level of 10^{-4}% (Figure 8). While th
nitude of $K_s(z,\lambda_o;h(\lambda))$ for the realistic h(λ) case (that is λ_o=620nm) m
ectly comparable to $K_{obs}(z,625nm)$, the correspondence with the observed shap
t the spectral response function may control the vertical structure of $K_{obs}(z$
arge degree. In particular, the correspondence of the vertical profile shapes
importance of the low level spectral structure of h(λ) far from the wav
terest.

As mentioned in the introduction, internal sources of light within the water column can produce reduced values of $K_{obs}(z,\lambda)$ similar to those observed (Figure 2). A conceivable mechanism for this process is sunlight induced pigment fluorescence. One can model this process by assuming that a fraction of the downwelling blue-green irradiance is absorbed and then re-emitted as downwelling red irradiance. This model is analogous to the stray light case previously introduced, where the fraction (r) of stray light becomes a depth independent fluorescence efficiency. Comparison of the results of the stray light computation and $K_{obs}(z,625nm)$ gives a hypothetical fluorescence efficiency of ~0.005%. Near this waveband, phycocyanin and phycoerythrin are the primary fluorescing pigments (e.g., Broenkow, et al.[14]). There are few field observations of fluorescence efficiencies in this waveband, but the magnitude of this estimate is not entirely unrealistic (e.g., Falkowski and Kiefer[15]).

It has been shown that the observed vertical structure of $K(z,\lambda)$ within the red spectral regions can be explained by using simple models of either a realistic irradiance sensor or by an internal source of light within the water column. No conclusive statement can be made concerning the cause of this vertical structure, but it is likely that a large portion of this vertical structure is due to the characteristics of the irradiance sensor in view of the large observed deviations from the assumed $K(\lambda)$ profile with the measured $h(\lambda)$ (Figure 8). With a larger, more complete data set (i.e., the inclusion of upwelling spectral irradiance, less incident irradiance variations, and a shallower chlorophyll maximum) it may be possible to make a more conclusive statement concerning the source of the observed vertical structure of $K_{obs}(z,\lambda)$ for these orange-red bands.

Using these calculations for a basis, it is possible that correction procedures can be developed if the spectral response function of the spectroradiometer is known. These procedures would be applied in ad hoc fashion, where the irradiance sampled outside the spectral region of interest would be subtracted from the entire sampled irradiance of the waveband. This would also require that the spectrum of $K(z,\lambda)$ be known a priori. Therefore an iterative scheme would be required. These approaches are presently being investigated.

Conclusions

Although the explanation for the observed vertical structure of $K(z,\lambda)$ in clear oceanic waters cannot be unambiguously determined, it is most likely that a substantial portion of the vertical structure for orange-red wavebands may be attributed to the characteristics of the irradiance sensor. Also, our model calculations suggest several factors which should be considered for the proper design of spectroradiometers. Model results indicate that great care should be made to insure that the finite blocking level of the spectral response function for the sensor be as small as possible (10^{-6}% or less). This may be a rather strict design requirement. Also, the maximum allowable half power bandwidth for a spectral irradiance sensor is shown to be ~10nm.

In addition, an estimate of the depth to which one can reasonably estimate $K(z,\lambda)$ can be derived. This depth occurs at nearly 7 optical depths for a spectroradiometer similar to that used from the R/P FLIP during ODEX. It should be emphasized that observed $K(z,\lambda)$ profiles are not only dependent upon space and time variability of the environment, but also upon the design and construction of the instruments used to measure the in situ spectral irradiance.

As discussed previously, the measurement of natural fluorescence in oceanic waters is receiving increasing interest. These discussions serve notice that spectral characteristics of the instrumentation can obfuscate the fluorescent source. Investigators are urged to carefully consider the spectral characteristics of the light field and their detectors when studying portions of the spectrum where there exist large changes in optical properties with wavelength.

Acknowledgments

This research has been supported by the Office of Naval Research under contract N00014-84-K-0322 to TDD. DAS would also like to acknowledge the support of the Office of Naval Research Graduate Research Fellowship program, which is administrated by the American Association for Engineering Education. Discussions with M.A. Blizard, A. Bratkovich, D.J. Collins, D.A. Kiefer, B.G. Mitchell, R.C. Smith, and L. Washburn are greatly appreciated.

References

1. Smith, R.C. and K.S. Baker, Optical classification of natural waters, Limnology and Oceanography, 23, 260-267, 1978.

2. Austin, R.W. and T.J. Petzold, Spectral dependence of the diffuse attenuation coefficient for irradiance, Proceedings of the Society for Photo-Optical Instrumentation Engineering, 489, Ocean Optics VII, 168-178, 1984.

3. Smith, R.C., C.R. Booth and J.L. Star, Oceanographic biooptical profiling system, Applied Optics, 23, 2791-2797, 1984.

4. Siegel, D.A. and T.D. Dickey, Observations of the vertical structure of the diffuse attenuation spectrum, submitted to Deep-Sea Research, 1986.

5. Smith, R.C. and K.S. Baker, the analysis of ocean optical data, Proceedings of the Society for Photo-Optical Instrumentation Engineering, 489, Ocean Optics VII, 119-126, 1984.

6. Smith, R.C. and K.S. Baker, Correction of underwater irradiance measurements for the accurate estimation of the diffuse attenuation coefficient, this volume, 1986.

7. Mueller, J.L., Multiple-wavelength method for filtering cloud shadows from oceanic spectral irradiance profiles, this volume, 1986.

8. Voss, K.J., J.W. Nolten and G.D. Edwards, Ship shadow effects on apparent optical properties, this volume, 1986.

9. Dickey, T.D., D.A. Siegel and A. Bratkovich, Optical, physical and biochemical variability in the northwest Pacific Ocean in the fall of 1982, Part III, Temporal evolution, to be submitted to Progress in Oceanography, 1986.

10. Gordon, H.B., Diffuse reflection of the ocean: the theory of its augmentation by chlorophyll-a fluorescence at 685nm, Applied Optics, 18, 1161-1166, 1979.

11. Topliss, B.J., Optical measurements in the Sargasso Sea: solar stimulated chlorophyll fluorescence, Oceanogolica Acta, 8, 263-270, 1985.

12. Jerlov, N.G., Marine Optics, Elsevier Scientific Publishing Company, Amsterdam, The Netherlands, 231p, 1976.

13. Melles Griot, Optics Guide 3, Melles Griot Optical Components, Irvine, California, 512p, 1985.

14. Broenkow, W.W., A.J. Lewitus and M.A. Yarbrough, Spectral observations of pigment fluorescence in intermediate depth waters of the North Pacific, Journal of Marine Research, 43, 875-891, 1985.

15. Falkowski, P. and D.A. Kiefer, Chlorophyll-a fluorescence in phytoplankton: relationship to photosynthesis and biomass, Journal of Plankton Research, 7, 715-731, 1985.